Journal of Alloys and Compounds 916 (2022) 165332

Contents lists available at ScienceDirect

Journal of Alloys and Compounds

journal homepage: www.elsevier.com/locate/jalcom

Synergistic effect of cobalt in hierarchical carbon nitride nanorods (HCNNR) with promising charge transfer rate by hole scavenger for stimulating solar H_2 production

Beenish Tahir[a], Muhammad Tahir[b,*], Mohammad Siraj[c], Amanullah Fatehmulla[d]

[a] School of Chemical and Energy Engineering, Universiti Teknologi Malaysia, UTM, 81310 Johor Bahru, Johor, Malaysia
[b] Chemical and Petroleum Engineering Department, UAE University, P.O. Box 15551, Al Ain, United Arab Emirates
[c] Department of Electrical Engineering, College of Engineering, King Saud University, P.O. Box 800, Riyadh 11421, Saudi Arabia
[d] Department of Physics and Astronomy, College of Science, King Saud University, P.O. Box 2455, Riyadh 11451, Saudi Arabia

ARTICLE INFO

Article history:
Received 27 March 2022
Received in revised form 3 May 2022
Accepted 5 May 2022
Available online 10 May 2022

Keywords:
Photocatalytic H_2 evolution
Carbon nitrides nanorods (CNNR)
Cobalt cocatalyst
Sacrificial reagents
Operating parameters

ABSTRACT

One-dimensional (1D) hierarchical carbon nitrides nanorods (HCNNRs) mediated by cobalt was designed and synthesized using a template free hydrothermal approach for improving solar light assisted H_2 evolution. The performance of 1D HCNNTs was significantly enhanced compared to bulk g-C_3N_4 due to larger active surface area, more visible light utilization and superior charge carrier along the unidirectional flow pathways. The 2% Co/HCNNRs (1D) exhibited excellent photocatalytic efficiency and optimal H_2 yield reached up to 620 μmol g^{-1}, which is 11.27 and 17.71 folds more than it was attained with pure HCNNR and bulk g-C_3N_4, respectively. This reveals that 1D structure helps to accelerate charge transport, whereas, Co works as a mediator to trap electrons, thus improving photocatalytic performance. The crucial operating parameters such as sacrificial reagents, feed concentration and catalyst loading were further optimized based on highest H_2 evolution. Interestingly, mass transfer, charge transfer and amount of photoinduced charges were greatly dependent on the operating parameters. Higher methanol and lower TEOA concentration were beneficial to yield highest photoactivity and stability. This work provides new approach to construct template free 1D nanorods and would be beneficial to enhance performance in other solar energy related applications.

© 2022 Elsevier B.V. All rights reserved.

1. Introduction

Photocatalytic H_2 evolution is a sustainable and economical process because it utilizes only light energy and produces environment biennial fuels to mitigate global warming effects [1]. In solar driven hydrogen production process, photocatalyst plays a crucial rule in achieving higher efficiency [2,3]. Layered polymeric graphitic carbon nitride (g-C_3N_4), among the various semiconductors, has increased enormous consideration in the field of metal free semiconductors due to its exceptional features such as low-cost, higher reduction potential, layered structure and chemical/thermal stability [4]. Nevertheless, it suffers restricted hydrogen production efficiency due to less exposed surface and weak absorbance of light and fast recombination of charge carriers [5].

In the recent advancement, various enhancement methods such as loading with metals and semiconductors coupling have been under exploration to exploit photocatalytic efficiency [6]. In heterojunction formation, g-C_3N_4/WO_3 composite with higher H_2 evolution has been reported [7]. In many other reports, Ag_2S/g-C_3N_4 [8], $LaVO_4$/g-C_3N_4 [9], and $ZnInS_4$/g-C_3N_4 [10] and $LaCoO_3$/g-C_3N_4 [11] have been explored for hydrogen production. Recently, we reported that metals as cocatalysts are more efficient to promote hydrogen instead of constructing heterojunction [12]. Therefore, it would be more beneficial to promote semiconductor efficiency by using low cost and small amount of metal loading compared to preparing semiconductors using expensive metals.

Numerous noble metals including Pt, Au, Ag and Ru are widely utilized as cocatalysts to tarp and transport charge carriers [13]. For example, Pt loaded over MOF was tested for improving hydrogen evolution [14]. Similarly, Au and Pt were loaded over TiO_2 to enhance H_2 evolution as these metals prevent charge carrier recombination [15]. Au was loaded over TiN to promote H_2 production by preventing charges recombination [16]. Ag-decorated P-doped g-CN_4

* Corresponding author.
E-mail addresses: muhammad.tahir@uaeu.ac.ae, bttahir@yahoo.com (M. Tahir).

https://doi.org/10.1016/j.jallcom.2022.165332
0925-8388/© 2022 Elsevier B.V. All rights reserved.

with improved H_2 evolution was observed [17]. However, noble metals practical application for industrial hydrogen production is hampered widely because of their high-cost and limited availability.

In replacement to noble metals, transition metals such as Ni, Co, Mn and Fe are considered very promising due to their low cost, earth abundant and reduceable characteristics [18–21]. Recently, we reported Ni and Ag loaded g-C_3N_4 with higher H_2 production because of prevented chargers recombination [22]. Similarly, Ni-cluster loaded g-C_3N_4 and Ni/TiO_2 were tested and observed improved charge separation, enabling more H_2 evolution [23,24]. Recently, Co is considered very promising due to its several characteristics such as loosely bounded d-electrons, provides active sites, and enables efficient trap of electron [25,26]. In addition, it provides higher stability to photocatalyst due to more carbon atom attachment to its active sites, thus hindering coke formation [27]. For example, we investigated Ni and Co loaded over TiO_2 for hydrogen production and observed boosted hydrogen production through steam reforming of phenol [28]. In another work, Co has been proven as an oxygen evolution cocatalyst coupled with CdS, whereas, Co-P work as hole collector to prevent charges recombination [29]. Co-loaded over TiO_2 was reported with higher H_2 evolution due to reducing the overpotential and facilitates the transfer of photoinduced electrons [30]. In another work, g-C_3N_4 efficiency was enhanced by loading with noble metal free CoP cocatalyst which enables efficiency for H_2 evolution [31]. Similarly, enhanced CO_2 reduction to CO was observed with Co single atom loaded photocatalysts, as it accelerates the separation of photogenerated charge carriers [32]. Therefore, further investigation of cobalt with noble metal free semiconductor would be beneficial to promote solar energy assisted hydrogen production.

In addition, structural development of graphitic carbon nitride have attracted many considerations due to their promising charge carrier separation, larger exposed active surface area, high aspect ratio, electron mobility along uniplanar direction, higher oxidation potential, more light penetration depth and quantum confinement effects [33–35]. In addition to several advantages, the performance of nanotextures can be further stimulated by loading with metals and coupling with other semiconductors. 3D g-C_3N_4 coupled with CdS was examined and reported obvious enhancement in H_2 evolution due to effectively increase in path length and shorten charge transport distance [36]. In another work, onion ring like g-C_3N_4 was coupled with Bi_3TaO_7 and found promising H_2 evolution efficiency [37]. Carbon nitride nanotubes doped with Ni, P and O were investigated and observed improvement in H_2 evolution due to facilitating the transfer of photogenerated electrons [38]. 3D micropore and carbon vacancy g-C_3N_4 was tested for enhanced CO_2 reduction and hydrogen production [39]. Ru-loaded 3D g-C_3N_4 with higher H_2 evolution was examined in another work [40]. Previously, we reported carbon nitride nanotubes for CO_2 reduction with significant improvement in photoactivity compared to bulk g-C_3N_4 [41]. In another work, carbon nitride nanorods were tested for CO_2 reduction and reported boosted photocatalytic activity under visible light [42]. Therefore, synergistic effect of cobalt and hierarchical one-dimensional (1D) carbon nitride would be promising to stimulate solar energy assisted H_2 evolution.

In this work, controlled structure and hierarchical carbon nitride nanorods (1D HCNNR) were synthesized using a facile template free single step thermal treatment method. The uniform dispersion of cobalt (Co) over 1D HCNNR was conducted using chemical reduction method through ultrasonic approach. The performance of Co-mediated HCNNRs was conducted in a continuous flow slurry photoreactor system illuminated with visible light irradiation. The role of structure and morphology was specifically investigated through different characterization techniques with different experimental validations. The performance of CNNR was obviously enhanced for H_2 evolution due to unidirectional transport of charges compared to bulk structure of g-C_3N_4. Loading cobalt, a significant enhancement in H_2 yield was noticed due to their good interface interaction. The influential effect of various parameters such as hole scavengers, sacrificial reagents, catalysts loadings, feed concentration and reaction time was further explored. The comparative performance was critically discussed in view of mass transfer effects, light penetration depths, adsorption/desorption limitations, availability of protons/holes and stability of alcoholic compounds. Furthermore, stability and recyclability in several cycles was conducted and results demonstrate potential application of nanotextures for developing cost-effective solar photocatalyst.

2. Experimental

2.1. Synthesis of g-C_3N_4 and 1D HC_3N_4 nanorods

The bulk and hierarchical carbon nitrides samples were synthesized using a hydrothermal approach. Bulk g-C_3N_4 is prepared through thermal polymerization of melamine as discussed previously [42]. The porous one-dimensional C_3N_4 was synthesized using mixture of melamine and urea, in which sample was heated at 550 °C with total time 2 h under air atmosphere. Typically, urea and melamine were added to crucible in different beds, in which urea was decomposed completely to produce gas, that was responsible to exfoliate g-C_3N_4 into 1D HC_3N_4 nanorods (HCNNR).

2.2. Synthesis of Co-loaded 1D HC_3N_4 nanorods

The Co-loaded HCNNRs samples were synthesized using combination of ultrasonic and impregnation methods. Typically, 0.5 g HCNNR in methanol (20 mL) was continuously stirred and kept under stirring for 6 h. Afterwards, cobalt nitrate (specific amount) was dissolved in 20 mL methanol and was gradually added to above suspension under stirring. The mixture was stirred for another 2 h and sonicated for 30 min to get exfoliated texture. Finally, the cobalt dispersed suspension was dried in oven at 80 °C overnight. Finally, fine powder was obtained after grinding and was given name as Co-loaded HCNNR. Different samples were prepared using different amounts of Co-loading (1, 2, 3 and 5 wt%) and was named as 1% Co/HCNNR, 2%Co/HCNNR, 3% Co/HCNNR and 5% Co/HCNNR, respectively. The schematic procedure for the preparation of g-C_3N_4, HCNNR and Co-loaded HCNNR samples is discussed in Fig. 1.

2.3. Characterization

The materials were characterized to investigate, structure, crystallinity, morphology, elements dispersion, light absorption and charge separation ability. XRD analysis was conducted using Bruker Advance D8 diffractometer to determine crystalline structure. Morphology analysis was conducted using SEM (Scanning electron microscopy) with Hitachi SU8020. The morphology was further conducted using HRTEM (High resolution transmission electron microscopy) with JEOL JEM-ARM 200 F. The element state and composition were obtained using X-ray Photoelectron Spectroscopy (XPS) with Axis Ultra DLD instrument. Light absorption and band gap energy was calculated using UV-3600 Plus Spectrometer. PL analysis was further conducted using HORIBA Scientific spectrometer (laser 325 nm). The Raman analysis was conducted using HORIBA spectrometer at wavelength 532 nm.

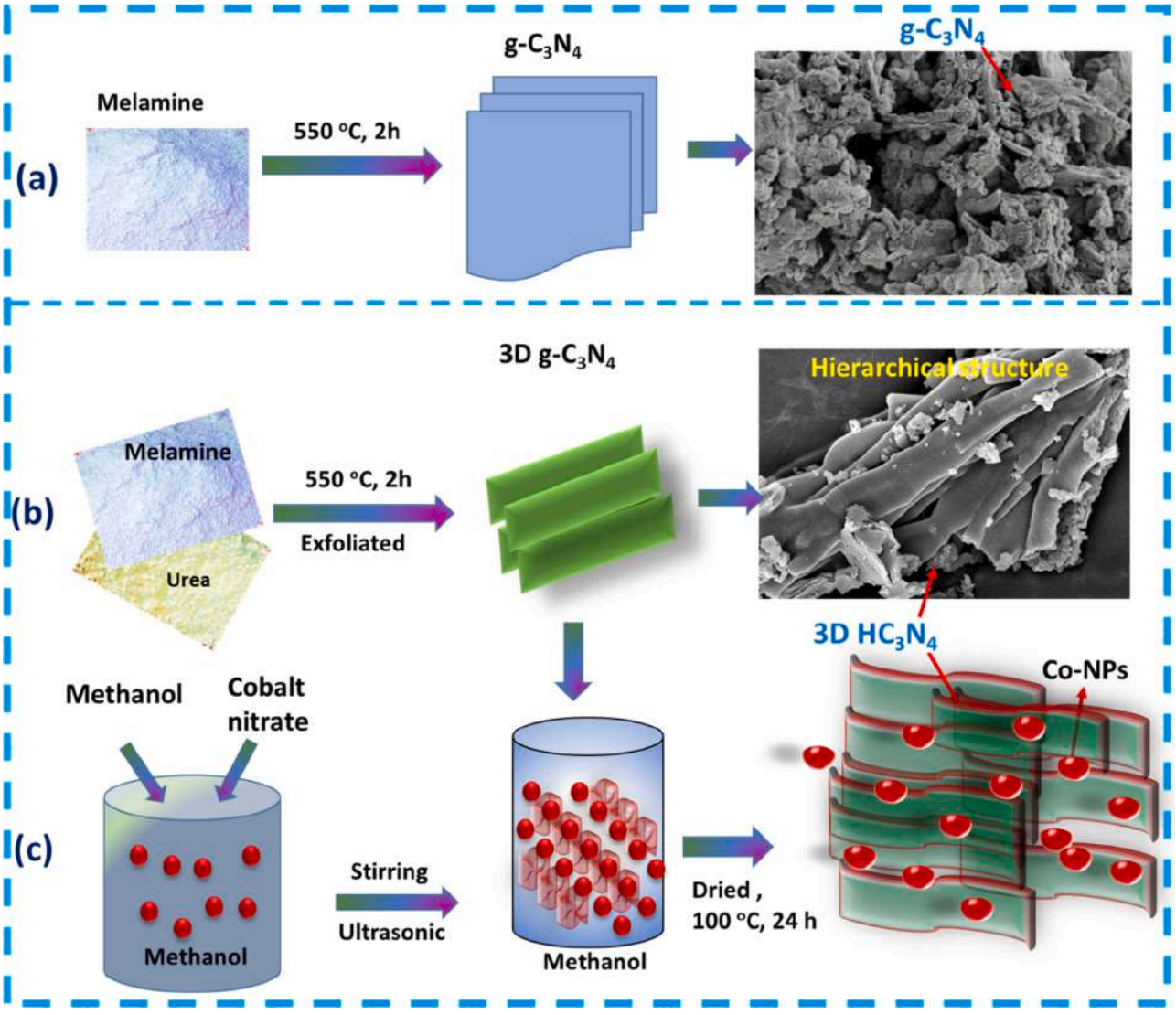

Fig. 1. Schematic illustration for the synthesis of bulk g-C_3N_4 and HCNNRs samples; (a) Synthesis of bulk g-C_3N_4, (b) Synthesis of HCNNRs and (c) synthesis of co-loaded HCNNRs.

2.4. Experimental photoactivity test

The H_2 evolution experiments were conducted in a cylindrical quartz glass photoreactor system. The reactor has total volume of 160 mL, whereas, 140 mL active volume was used for all the experiments. The light source used for photoactivity test was a visible light source with power 35 W HID Xenon. The experiments were performed without using UV-cut filters. Before starting experiment, 100 mg powder photocatalyst was dispersed inside reactor containing 140 mL aqueous solution of water-sacrificial reagent. The reactor and piping system were cleaned using continuous flow of nitrogen, whereas, flow of nitrogen was constantly flowing to remove hydrogen from the reactor and was stored using sampling bags. The parameters investigated were catalyst loading, sacrificial reagents, concentration, irradiation time and reusability in cyclic runs. Methanol, glycerol and triethanolamine sacrificial reagents with their different concentrations (vol%) ranging 2–10 vol% were investigated. The catalyst was loaded in the range of 50–200 mg and the effect of mass transfer was investigated. Similarly, effect of different times was investigated for both continuous hydrogen evolution and for cyclic stability. The gas product was tested on continuous interval of 60 min using gas analyzer and gas chromatography as discussed previously [2,42].

3. Results and discussion

3.1. Characterization

The XRD results of g-C_3N_4, HCNNR and Co loaded HCNNR are shown in Fig. 2(a). Two diffraction peaks at 2θ of 12.76° and 27.29° were obtained for g-C_3N_4, indexed to the (1 0 0) and (0 0 2) planes, respectively. These peaks correspond to tri-s-triazine segments of basic in-plane periodic structure and interlayer stacking of aromatic rings for g-C_3N_4 [43]. When g-C_3N_4 was converted to 1D HCNNR, there was no change in the crystalline structure, which confirms successful fabrication of nanorods of g-C_3N_4 without any change in crystalline structure. When Co was loaded over 1D HCNNR, the crystalline plane of (0 0 2) was slightly altered with 2θ of 27.39°, which confirms successful fabrication of Co-loaded 1D HCNNT using facile single step hydrothermal approach and similar results are reported previously [36].

The Raman analysis for g-C_3N_4, HCNNR and Co-loaded HCNNR was further conducted to understand the successful fabrication of nanotexture and their good interface interaction and results are presented in Fig. 2(b). For pure g-C_3N_4, Raman peaks were observed at 469.8 cm^{-1}, 704.4 cm^{-1}, 977.7 cm^{-1}, 1115.4 cm^{-1}, 1480 cm^{-1} and 1619.4 cm^{-1}, corresponding to polymeric structure of graphitic

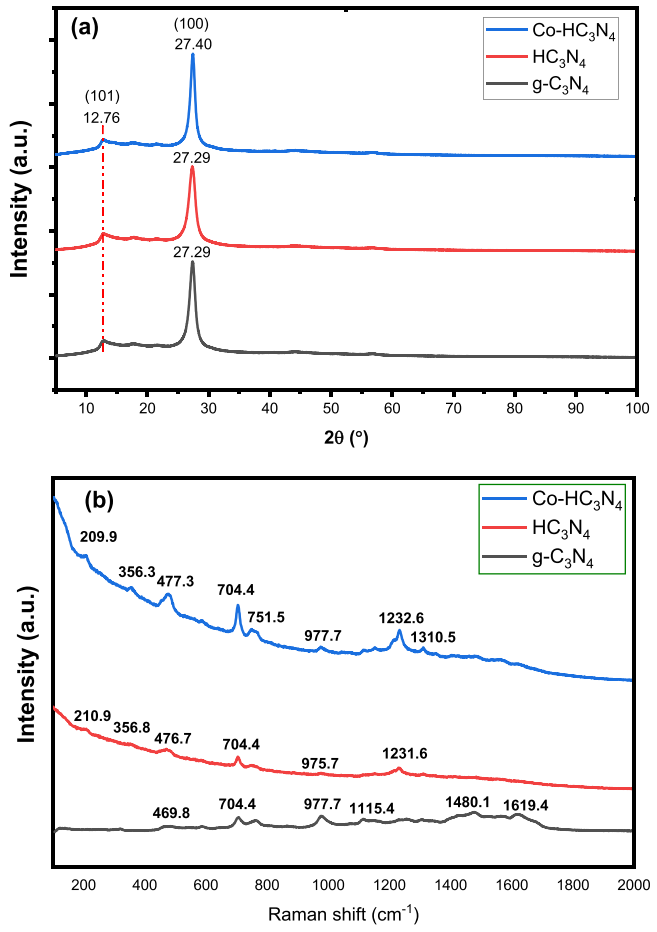

Fig. 2. (a) XRD analysis of g-C_3N_4, HCNNR and Co/HCNNR samples, (b) Raman analysis of g-C_3N_4, HCNNR and Co/HCNNR samples.

carbon nitride. For 1D HCNNR, Raman peaks were observed at 210.9 cm^{-1}, 356.8 cm^{-1}, 476.7 cm^{-1}, 704.4 cm^{-1}, 975.7 cm^{-1}, and 1231.6 cm^{-1}. Comparatively, one new peak was observed at 210.9 cm^{-1}, whereas, other peaks were somewhat altered due to complete decomposition of melamine to polymeric structure. When Co was loaded over 1D HCNNR, all the peaks were observed, whereas, their positions was somewhat altered due to good interaction with cobalt. All such observations are in close agreement with the results obtained by XRD analysis.

The change in structure and morphology of g-C_3N_4, 1D HCN nanorods and Co-loaded 1D HCNNR was inspected using FESEM as shown in Fig. 3(a-d). Fig. 3(a) shows closely packed non-uniform sheets of g-C_3N_4 with irregular structure using thermal treatment of melamine under air atmosphere. Fig. 3(b-c) shows uniform size and one-dimensional carbon nitride nanorods. This confirms successfully structured 1D HCNNR using template free thermal treatment of melamine in the presence of gases released from the decomposition of urea. When Co-was loaded over HCNNR through ultrasonic approach, exfoliated and mesoporous structure of HCNNR was achieved as shown in Fig. 3(d). This would be beneficial to promote light utilization with higher distribution of Co for fast charge carrier separation.

The structure of Co-loaded 1D HCNNR was also examined using TEM and structural developments are depicted in Fig. 3(e-f). The TEM image in Fig. 3(e) shows obvious g-C_3N_4 sheets with rod like structure. The layered CN has obvious 1D rods with uniform size and shape as depicted in Fig. 3(f). All these observations approve successful fabrication of 1D HCNNR with controlled structure using single step thermal treatment. EDX mapping analysis was further conducted to assess elements distribution and results are discussed in Fig. 4. Fig. 4(a) shows morphology of HCN nanosheets loaded with Co. Fig. 4(b) shows EDX peaks of C, N, O and Co. The EDX mapping distribution of Co, C, N and O is further illustrated in Fig. 4(c) with their uniform distribution. Furthermore, color distribution in Fig. 4(d-g) shows the presence of C, N, Co and O, respectively. Thus, successful fabrication of Co/1DHCNNR composite can be obtained using facile hydrothermal method.

Fig. 5 shows XPS analysis of Co-loaded HCNNR to understand elemental state and their compositions. Fig. 5(a) shows C 1 s high resolution spectrum with 284.6 and 288.1 eV binding energies, ascribed to C-C and N-C=N, respectively [44]. In the resolution spectrum of Co 2p in Fig. 5(b), four peaks were obtained, which were positioned at binding energies 780.6, 787.2, 797.2 and 802.3 eV. Similarly, 780.6 and 797.2 eV binding energies ascribed to spin orbits Co $2p_{3/2}$ and Co $2p_{1/2}$, respectively, indexed to Co^{2+} [45]. The two peaks at 787.2 and 802.3 eV are satellite peaks, which further confirms the existence of cobalt as oxide state [19]. Fig. 5(c) shows N1s spectrum with 397.7, 398.9 and 401.3 eV binding energies, ascribed to C-N=C, N-$(C)_3$ and C_2-NH, respectively [44]. Fig. 5(d) shows O 1 s spectrum with binding energies 529.6 and 532.3 eV, belonged to lattice oxygen and absorbed water and oxygen vacancies produced within the g-C_3N_4 structure. All these results conclude Co loaded over HCNNR as a Co^{2+}, whereas, presence of oxygen vacancies was also observed, which will be beneficial to promote charge carrier separation.

The optical properties of g-C_3N_4, HCNNR and Co-loaded HCNNR was further conducted using UV–vis DRS and results are shown in Fig. 6(a). Using g-C_3N_4 and 1D HCNNR, there was not much difference in UV–visible light absorption spectra. This was obviously due to no change in crystalline structure of the samples. When Co was loaded to HCNNR, light absorption was slightly increased due to visible light response of the cobalt. For g-C_3N_4, HCNNR and Co/HCNNR, Kubelka–Munk (K-F) was used to calculate band gap energy as shown in Fig. 6(b). The energy band gap of 2.83, 2.84 and 2.83 eV were estimated for g-C_3N_4, HCNNR and Co-loaded HCNNR samples, respectively. Previously, 2.80 eV band gap for g-C_3N_4 , synthesized through thermal decomposition of melamine at 600 °C for 2 h, was obtained [46]. Similarly, 2.79 eV band gap energy was reported for 2D g-C_3N_4, synthesized through thermal polymerization of melamine at 550 °C for 4 h [8]. Recently, increased band gap of g-C_3N_4 (2.71 eV) was obtained by converting into 3 DOM g-C_3N_4 (2.76 eV) [36].

The g-C_3N_4, HCNNR and Co-loaded HCNNR charge carrier separation was further investigated using PL as shown in Fig. 6(c). Higher PL intensity was obtained with g-C_3N_4 due to more recombination of charge carriers [33]. However, a diminished peak intensity was observed with 1D HCNNR, which is ascribed to less charge's recombination compared to g-C_3N_4. This shows 1D structure has more potential to increase life of electrons and holes. Recently, a lower PL intensity of 3DOM g-C_3N_4 compared to bulk g-C_3N_4 has been reported due to quantum size effect [36]. A further weakened PL intensity was noticed when Co was loaded over HCNNR, evidently efficient charge carrier separation and transportation. This reveals, cobalt is not only beneficial to increase active sites but also works as mediator to trap and transport electrons, which results in their lower recombination rate. In many articles reduced in PL intensity has been reported using metals as cocatalysts such as NiO/g-C_3N_4 [47], Ni-Ag/g-C_3N_4 [22], and Ag/g-C_3N_4 [43]. All these findings confirm that not only metals but structural alternation is beneficial to hinder charges recombination rate. Also, synergistic effect of metal and morphology has significant effect to weaker PL intensity, thus, enabling proficient charge carrier separation.

The PL charge separation analysis can also be further investigated using several other techniques. For example, Peng et al., [31]

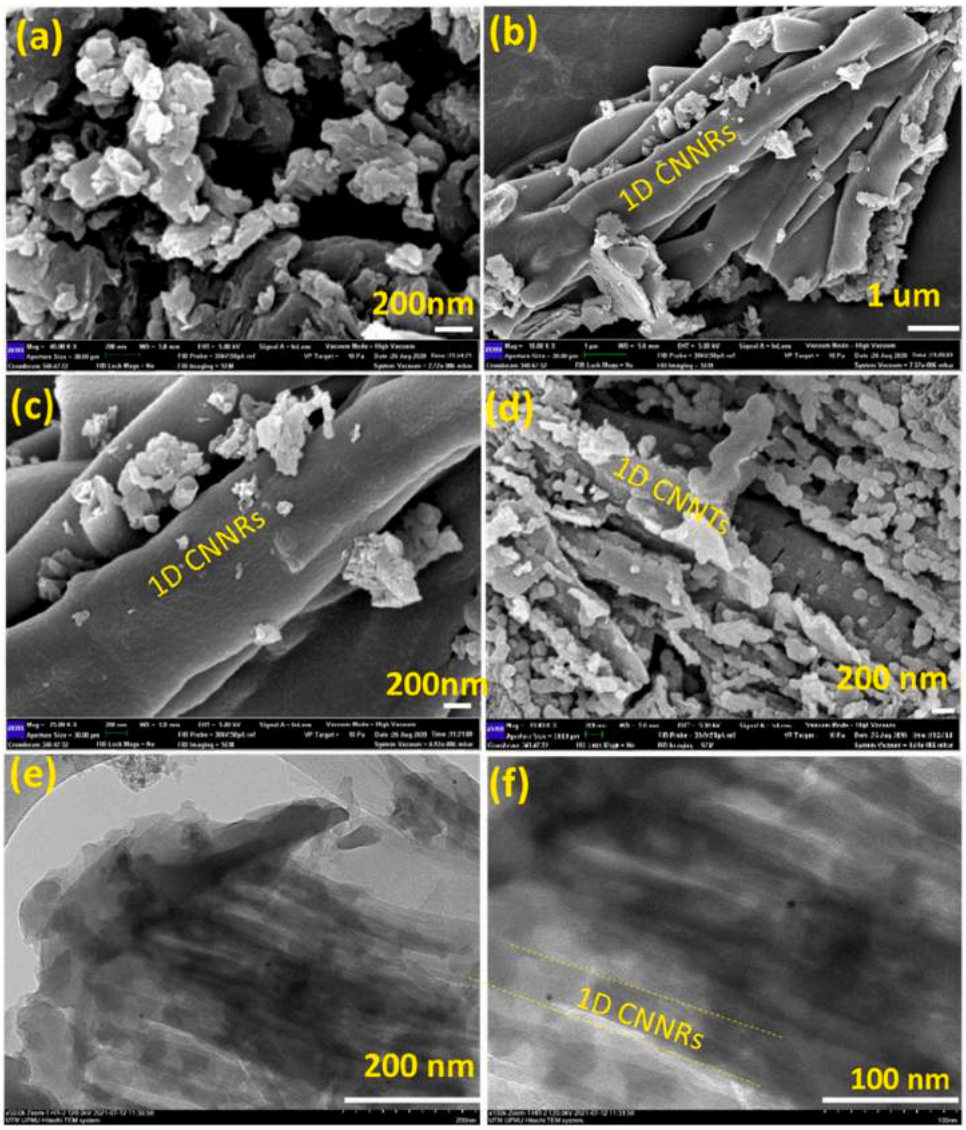

Fig. 3. (a) SEM image of g-C_3N_4, (b-c) SEM images of 1D HCNNRs, (d) SEM image of Co-loaded HCNNR, (e-f) TEM images of Co-loaded HCNNR with uniform size and shape.

reported higher photocurrent intensity of CoP/g-C_3N_4 compared to bulk g-C_3N_4 which proves cocatalysts as a promising source for the separation and transfer of photoinduced electron and holes. In another development, PL analysis was compared with photocurrent tests and observed higher photocurrent density of nitrogen vacancy rich g-C_3N_4 than using bulk g-C_3N_4. It was concluded that N vacancy modified g-C_3N_4 improves charges separation rate, resulting in higher photocurrent density and photocatalytic efficiency [35,48].

3.2. Photocatalytic hydrogen production

3.2.1. Effect of Co-loading

The performance of different graphitic carbon nitride materials such as bulk g-C_3N_4, one-dimensional carbon nitride nanorods (CNNRs) and Co-loaded CNNRs was examined using glycerol as a hole scavenger (sacrificial reagents) under visible light and the results are shown in Fig. 7. Using bulk g-C_3N_4, highest 35 µmol g^{-1} H_2 yield was attained, whereas, it was boosted to 55 µmol g^{-1} with 1D nanorods of HCN. This significant enhancement in H_2 yield can be ascribed to transfer of electrons in one dimensional along the length of rods, enabling their effectual utilization during protons reduction process as illustrated in Fig. 7(b-c). Recently, 3D g-C_3N_4 was examined for H_2 evolution and observed significantly improved photoactivity due to non-radiation pathway which enables improvement in charge separation [36]. Mesoporous g-C_3N_4 with higher H_2 evolution was reported due to higher charges migration [49].

The performance of HCNNR was further investigated using different Co loading amounts of 1–5 wt% (Fig. 7a). Loading 1 wt% Co into HCNNR, H_2 of 320 µmol g^{-1} was produced, nearly 5.82 times more than using pure HCNNR. Using 2 wt% Co-loaded over HCNNR, highest H_2 yield of 620 µmol g^{-1} was attained. This amount of H_2 yield over 2% Co/HCNNR is 11.27 and 17.71 folds more than it was attained with pure HCNNR and bulk g-C_3N_4, respectively. This augmented photoactivity can be linked to several factors such as unidirectional flow of electrons with boosted charges separation by Co, higher active sites, oxygen vacancies and more visible light utilization [50,51]. Recently, nitrogen vacancy g-C_3N_4 was investigated and observed 5.9 folds higher H_2 evolution compared to bulk g-C_3N_4 due to higher surface area, stronger light response and improved migration and separation of charge carriers [35]. Similarly, higher H_2 evolution was achieved over mesoporous g-C_3N_4 having nitrogen defects due to increased charge carrier separation [48,52]. However, when 3 and 5 wt% Co-loading was used, H_2 productivity was

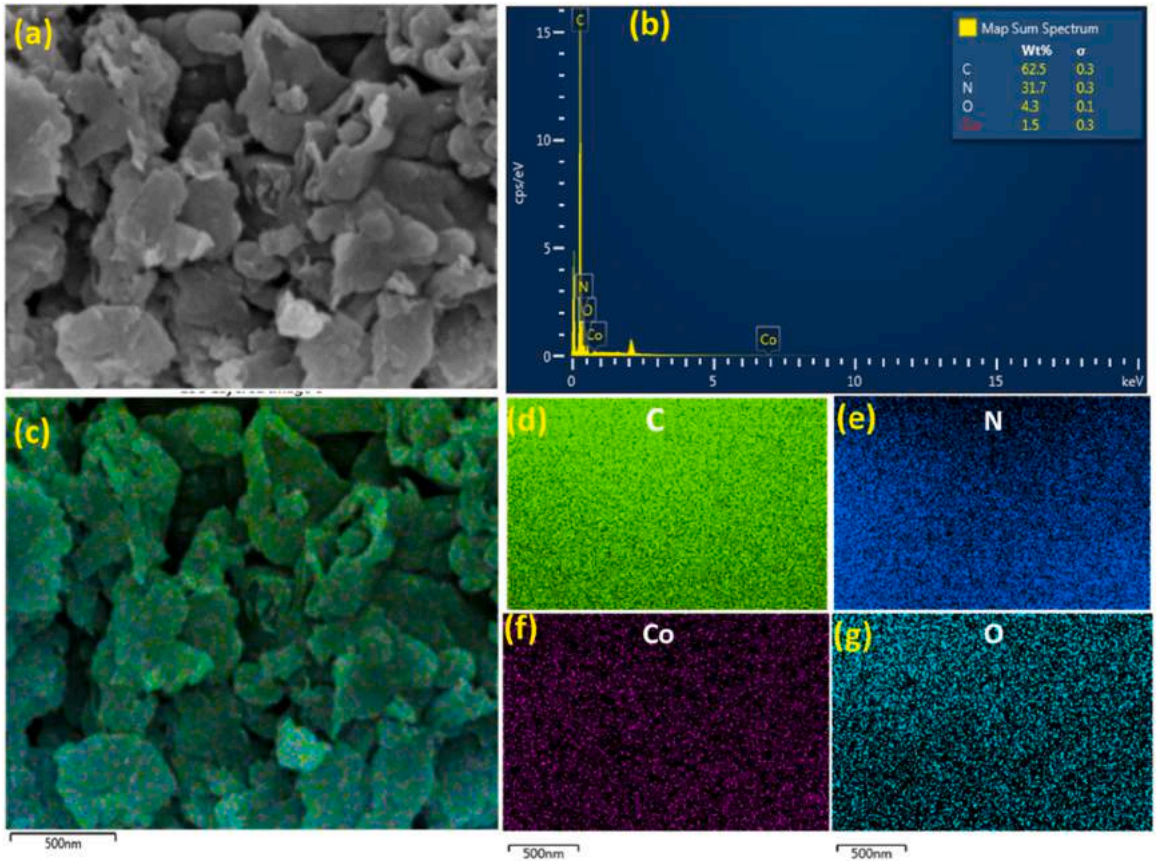

Fig. 4. SEM and EDX mapping analysis of Co-loaded HCNNR; (a) SEM of Co/HCNNR, (b) EDX plot, (c) EDX mapping of elements distribution, (d-g) color images for C, N, Co and O.

gradually declined. Several possibilities exit in these decreasing trends such as aggregation of extortionate loading quantity within the g-C_3N_4 hollow nanorods and also prevents more light harvesting over the active sites [19].

Fig. 7(b-c) shows charge transfer illustration over 2D g-C_3N_4 and 1D nanorods for photocatalytic H_2 evolution. Using 2D sheets, electrons have to travel longer distance to react with protons for hydrogen production. In addition, due to production of electrons and holes, there would be possible recombination of photoinduced charges, resulting in lower hydrogen production. Furthermore, due to compact sheets, there is less penetration of light, resulting in lower hydrogen production. When, 2D g-C_3N_4 was converted to 1D nanorods, there was efficient transport of charges along the length of nanorods, providing two possibilities, less charges recombination and more availability for H_2 evolution. All such results and findings confirm that alternation of structure and morphology have significant effect on photocatalytic efficiency enhancement.

3.2.2. *Effect of sacrificial reagents*

The photocatalyst performance is greatly dependent on the sacrificial reagent due to the challenges of charge carrier recombination and lower number of protons produced during water oxidation. Therefore, to further understand the effectiveness of 1D Co/HCNNR photocatalyst, the role of different hole scavenger such as glycerol, methanol and triethanolamine (TEOA) were investigated and their results are shown in Fig. 8. Fig. 8(a) shows performance comparison of different sacrificial reagents in the presence of 2% Co/HCNNR while keeping all other variable constant. Using pure water, H_2 yield of 50 µmol g^{-1} was produced, whereas, with 5 vol% glycerol, 12.4 folds (620 µmol g^{-1}) higher H_2 amount was obtained. The H_2 yield of 920 and 745 µmol g^{-1} were produced using methanol and TEOA, respectively. Comparatively, highest H_2 yield was produced with methanol as the sacrificial reagent, which is 1.23, 1.48 and 18.4 folds higher than it was evolved by using TEOA, glycerol and water, respectively.

The findings of this work for H_2 evolution using various sacrificial reagent can be discussed based on various hypothesis. In general, sacrificial reagent traps holes and also useful to produce electrons, resulting in excessive availability of protons (H^+) and electrons (e^-) for the reduction reaction of H_2 production. Thus, lower H_2 yield with H_2O can be ascribed due to less protons (H^+) production but more electron-hole pairs recombination. On the other hand, higher production of H_2 with methanol and TEOA than it was evolved using glycerol, probably due to more adsorption of these molecules over the catalyst surface having active sites [53]. Previously, it has been investigated that TEOA with g-C_3N_4 has higher H_2 yield compared to methanol, ethanol, glycerol and many other sacrificial reagents. This was suggestively due to higher stability of π conjugated structure of amine rich g-C_3N_4 by the effective binding of TEOA over the photocatalyst surface. Furthermore, TEOA improves photocatalyst dispersion and consumes photogenerated holes, enabling obviously enhanced H_2 productivity [54]. In another development, Ru/g-C_3N_4 was tested for photocatalytic H_2 evolution using glycerol and methanol hole scavengers. The H_2 yield with highest quantity was achieved using methanol due to proficient methanol molecules attachment over the catalyst active sites [40].

The concentration of different sacrificial reagents was further investigated to evaluate the performance of Co/HCNNR photocatalyst. The glycerol, methanol and TEOA concentrations of 2–10 vol % in water were prepared and were tested using 100 mg of photocatalyst. Fig. 8(b) shows H_2 evolution rate with glycerol 2, 5 and 10 vol% in water. Using small amount of glycerol (2 vol%), H_2 production of 265 µmol g^{-1} was produced, approximately 5.3 folds higher than using only water. This obvious enhancement was due to

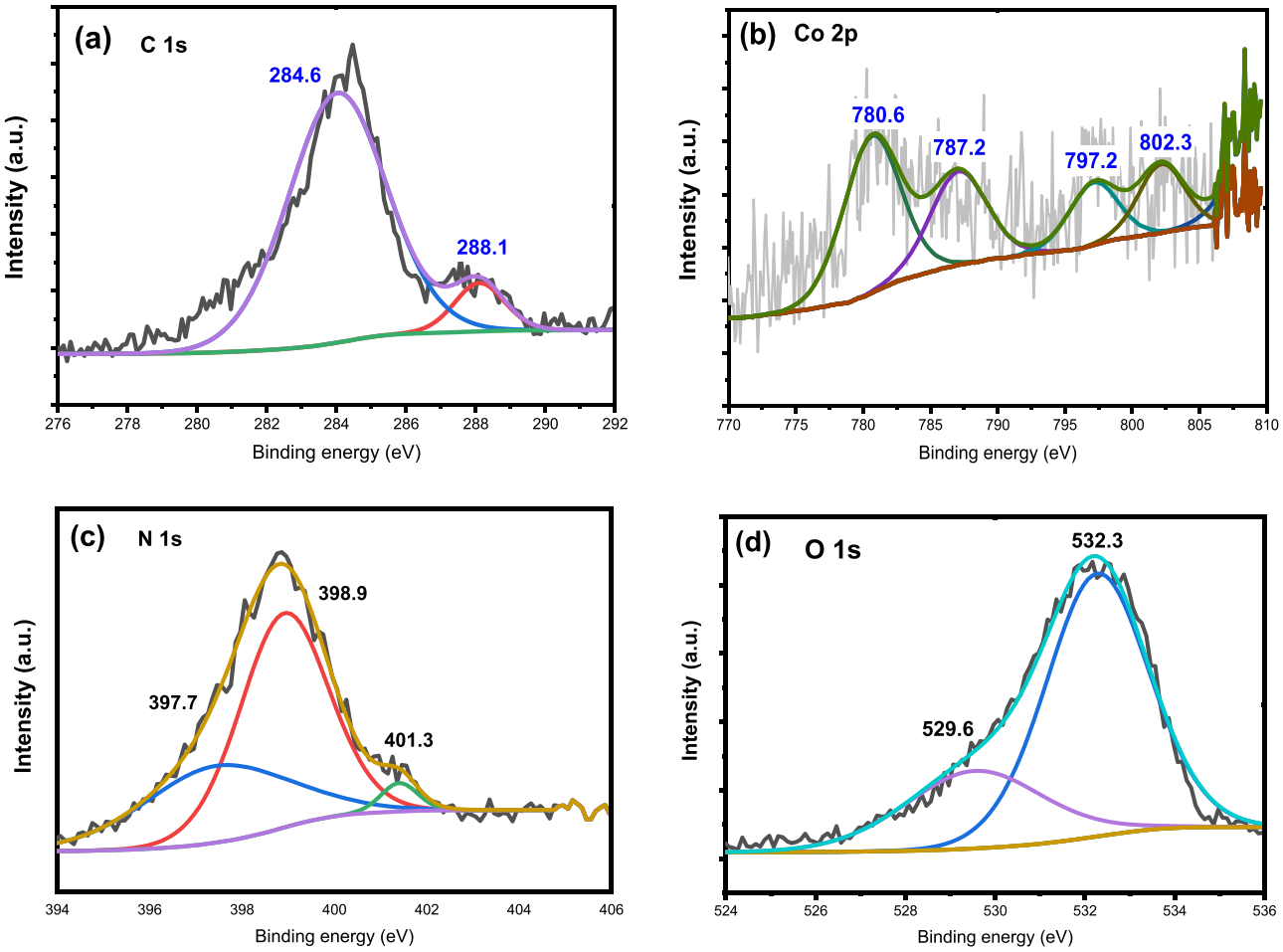

Fig. 5. XPS analysis of Co/HCNNR; (a) C 1s, (b) Co 2p, (c) N 1s, and (d) O 1s.

more production of protons (H^+) with consumption of holes (h^+), thus, enabling to prolong life of charge carriers. The amount of H_2 was further upgraded to 620 and 1005 μmol g^{-1}, when glycerol concentration was increased to 5 and 10 vol%, with H_2 increment of 12.4 and 20.1 folds while keeping all the parameters identical. This augmented H_2 production with increasing glycerol concentration was probably as a result of more absorption of molecules on the active sites of the photocatalyst. This reveals, glycerol is an important sacrificial reagent to promote photocatalyst performance.

Fig. 8(c) shows the effect of methanol concentration on the 1D Co/HCNNR photocatalyst performance at different irradiation time. Using H_2O, trivial quantity of H_2 was evolved, noticeably improved when methanol of 2 vol% was added to reactor system. This was obviously due to more production of protons (H^+) and electrons (e^-) with prolonged life time of photogenerated electron and hole pairs. When concentration was increased to 5 vol%, a significant enhancement of H_2 yield over the entire irradiation time was achieved, supposedly due to more protons and electrons production over the photocatalyst surface. However, when concentration was increased to 10 vol%, different trends were observed, whereas, initially, more H_2 production was observed at the start of reaction, however, it was reached to lower values than 5 vol% after 60 min of irradiation time. These observations can be explained based on several factors such as mass transfer, attachment of reactants over the active surface and saturation of catalyst active sites with side products. With increasing methanol concentration to 10 vol%, probably active sites were saturated with methanol due to its good attachment with catalyst surface, thus, activating reforming reaction for the production of other products such as CO and CH_4 instead of only H_2 [55]. Thus, hydrogen production was increased with increasing methanol initial concentration, however, more investigations are required to further understand the role of Co and HCNNR for such observations.

Fig. 8(d) shows the performance of 1D Co/HCNNR photocatalyst with various vol% of TEOA under different irradiation times. Interestingly different results were obtained by varying TEOA concentration over the reaction time. Using 2 vol% TEOA, initially, lowest amount of H_2 was produced until reaction time of 1 h, however, H_2 yield was significantly improved with increasing reaction time. When the TEOA concentration was increased to 5 and 10 vol%, initially, H_2 yield was increased until reached to 1 h and then it was lower than 2 vol% TEOA. By comparing performance based on 2 h irradiation time, H_2 yield was increased in order of 2 vol% TEOA > 5 vol% TEOA > 10 vol% TEOA > H_2O. These findings can be explained based on several hypothesis and possibilities. Using pure water, lower amount of H_2 yield was obviously due to lower amount of proton production with more charges recombination rate. Initial increasing of H_2 yield by varying TEOA concentration was probably due to less dispersion of highly viscous TEOA in water. Thus, with increasing concentration, more TEOA was attachment to catalyst active sites, thus, enabling to enhance H_2 yield. Conversely, decreased in H_2 yield with higher concentration after 2 h was evidently more TEOA attachment over the active sites due to its good adsorption capacity over g-C_3N_4 compared to methanol and glycerol, thus, H_2 yield was declined. Another possible reason would be less light penetration at higher TEOA concentration due to its higher viscosity and also possibility of other products production such as CO and CH_4 due to the activation of reforming reaction [55]. However, further investigations are required to explore about sacrificial

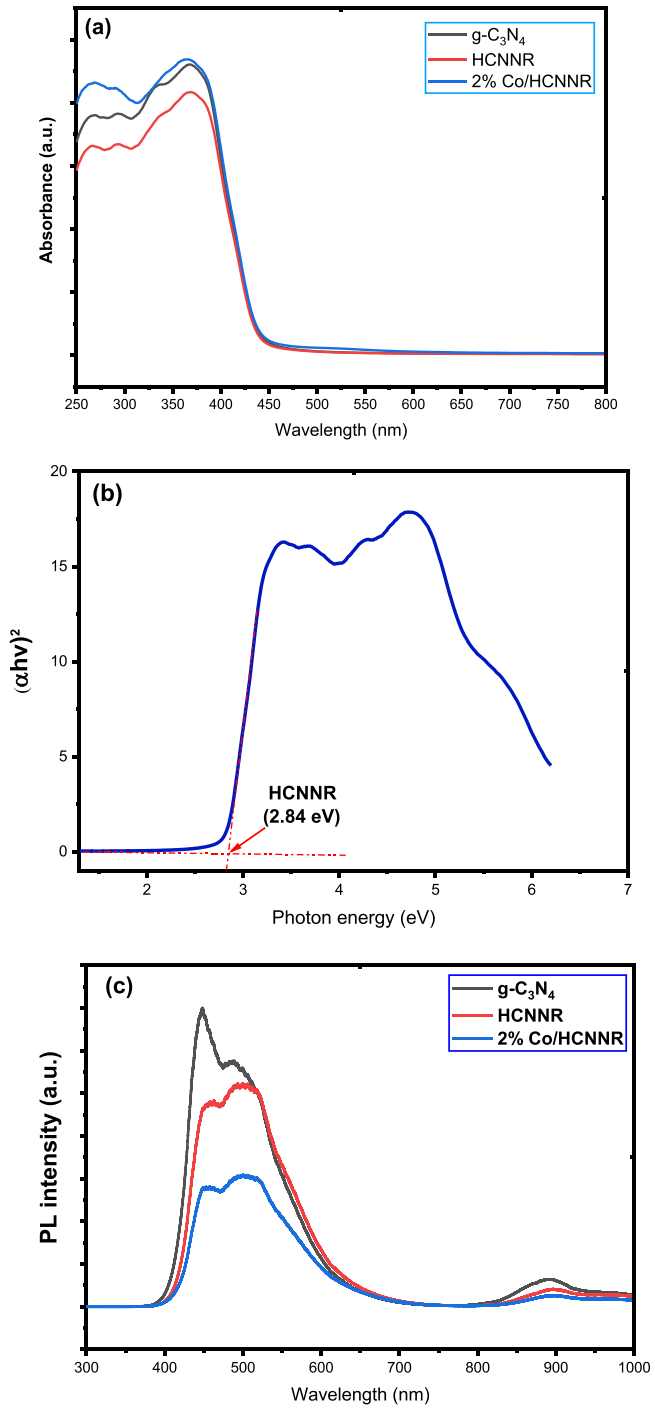

Fig. 6. UV–vis DRS of g-C_3N_4, 1D HCNNR and Co-loaded HCNNR samples, (b) Estimation of band gap energy for HCNNR; (c) PL analysis of g-C_3N_4, 1D HCNNR, and Co-loaded HCNNR samples.

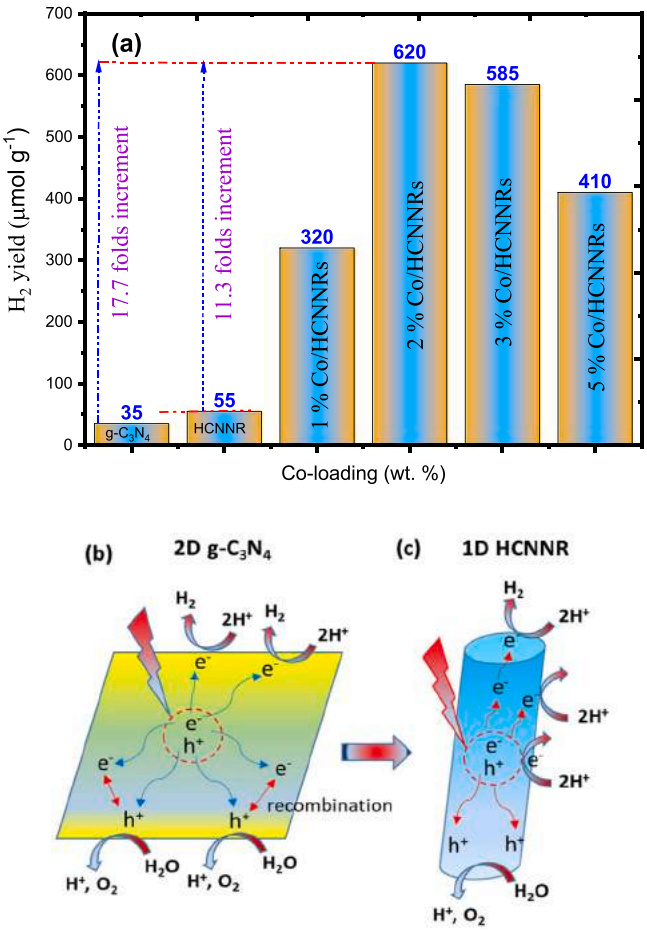

Fig. 7. (a) Comparison of H_2 production over g-C_3N_4 and HCNNR and effect of Co-loading on HCNNR using glycerol as the sacrificial reagent; (b-c) Schematic illustration of charge transfer in bulk and 1D HCNNR.

reagents role and their concentration on the photocatalyst performance. Thus, both types of sacrificial reagents and their concentrations are crucial to investigate to maximize the photocatalyst performance.

3.2.3. *Effect of catalyst loading*

In photocatalysis process, production of charge carriers and the reactants i.e., water and sacrificial reagent attachment over the photocatalyst active surface are significant features to be considered to comprehend mechanism of H_2 production. For this purpose, performance of Co/HCNNR photocatalyst was further investigated by varying loading amounts from 50 to 200 mg using TEOA hole scavenger. Fig. 9(a) shows the yield of H_2 (μmol) at different catalyst loading and reaction times. Using photocatalyst loading of 50 mg, trivial H_2 yield was evolved, obviously attributable to less availability of catalyst surface for photocatalytic reaction. When catalyst amount was increased further to 100, 150 and 200 mg, continuous increment in H_2 evolution was detected over the entire irradiation. These results can be clarified by considering two factors; with the increase of photocatalyst loading, more catalyst active surface availability for the attachment of TEOA and excessive generation of photoinduced charges due to more light utilization. Therefore, more production of proton (H^+) and electrons were obtained with increasing catalyst loading, resulting in more H_2 production through proton reduction process.

The role of catalyst loading was further examined in terms of per unit weight of hydrogen produced (μmol g^{-1}) and the results are discussed in Fig. 9(b). Interestingly different patterns of H_2 yield were obtained using units of μmol g^{-1} compared to H_2 yield in units of μmol as discussed previously. Using catalyst of 50 mg, less H_2 (μmol g^{-1}) amount was obtained due to less availability of active surface area. However, highest H_2 yield (μmol g^{-1}) was obtained using 100 mg of catalyst loading. This was evidently due to optimized surface-active sites available to maximize the rate of reaction. When the catalyst loading was increased to 150 and 200 mg, the H_2 yield was decreased due to the several possible reasons. With increasing catalyst loading above the optimal value, it provides hindrance for the penetration of light irradiation inside the slurry dispersion system. Besides, with excessive catalyst loading, only

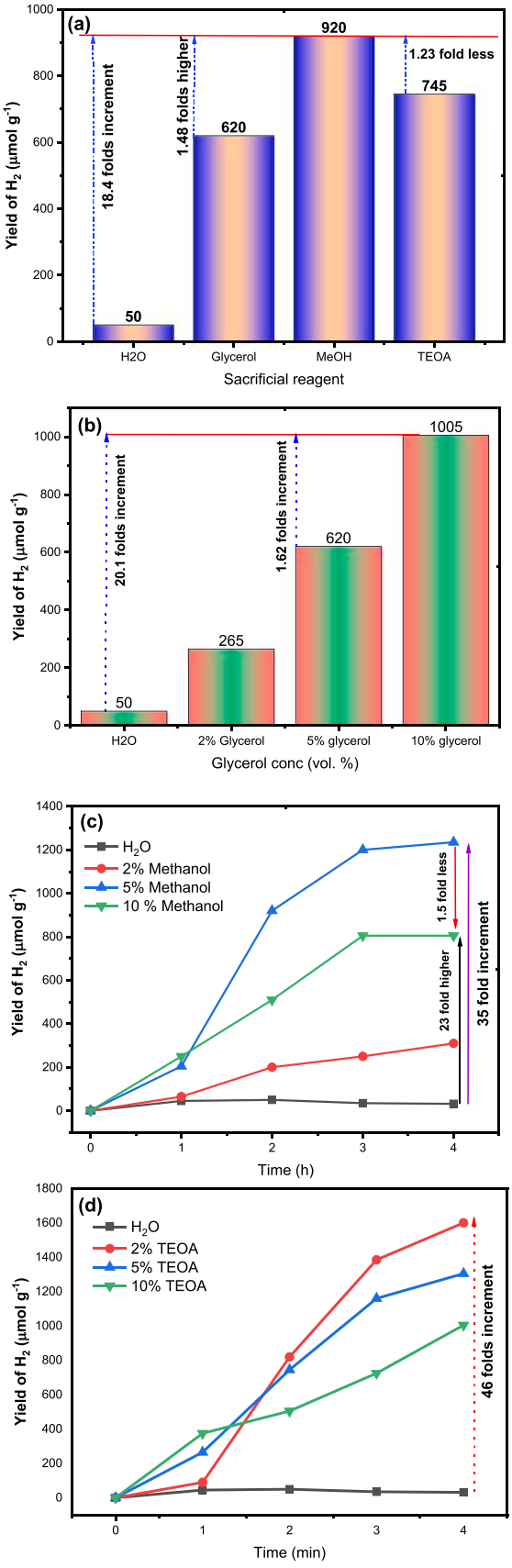

Fig. 8. (a) Effect of glycerol, methanol and TEOA sacrificial reagent on H_2 evolution, (b) Effect of glycerol concentration for H_2 evolution, (c) Effect of methanol concentration for H_2 evolution, (d) Effect of TEOA concentration for H_2 evolution.

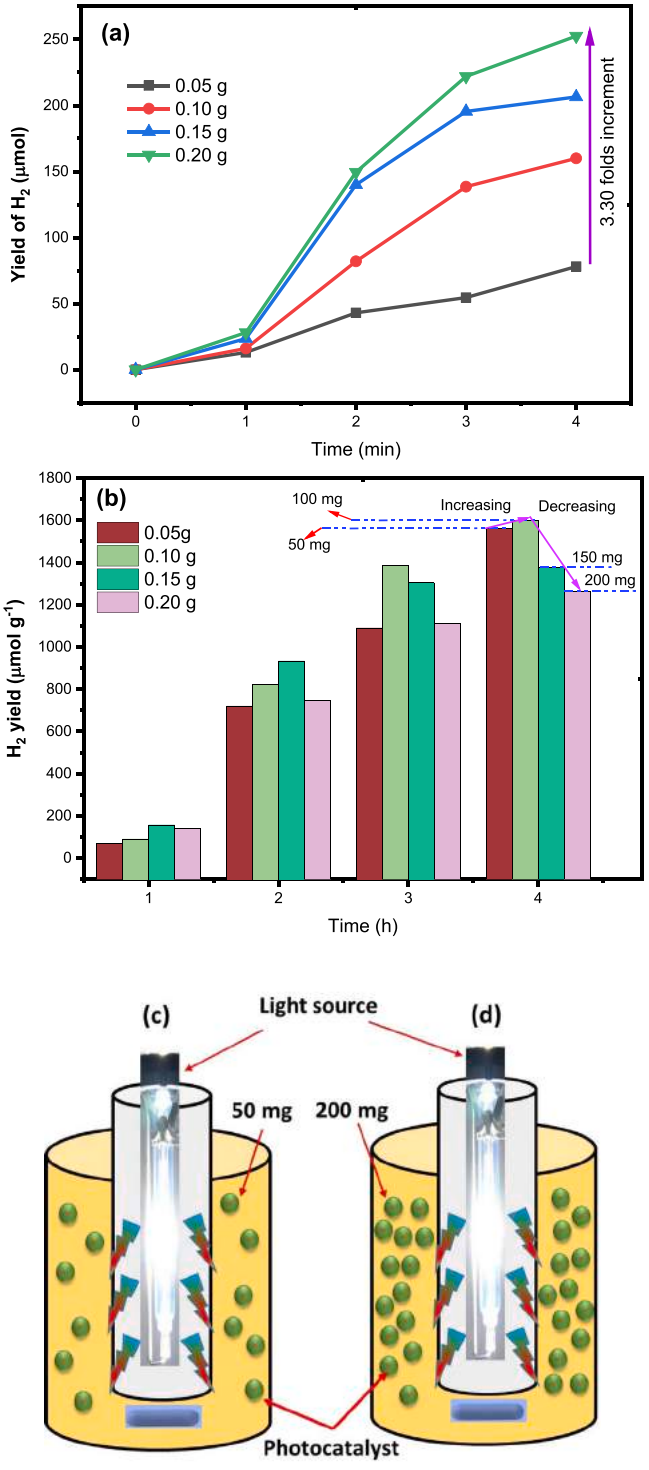

Fig. 9. Effect of 2% Co/HCNNR catalyst loading on hydrogen production using 2% TEOA sacrificial reagent (a) H_2 yield in µmol; (b) H_2 yield in µmol g^{-1}; (c-d) Schematics illustration of catalyst dispersion inside photoreactor system.

small portion of catalyst will be exposed to light irradiation, thus, yield of H_2 per unit mas of catalyst will be reduced. Furthermore, H_2 yield was different with various irradiation times. For the first 2 h, highest H_2 yield was obtained using 150 mg, however, beyond 2 h of reaction time, 100 mg was the optimized amount to maximize H_2 productivity. This can be justified based on two hypotheses. Initially, at the start of reaction, catalyst was not uniformly dispersed and there was good channeling for the penetration of light irradiation to

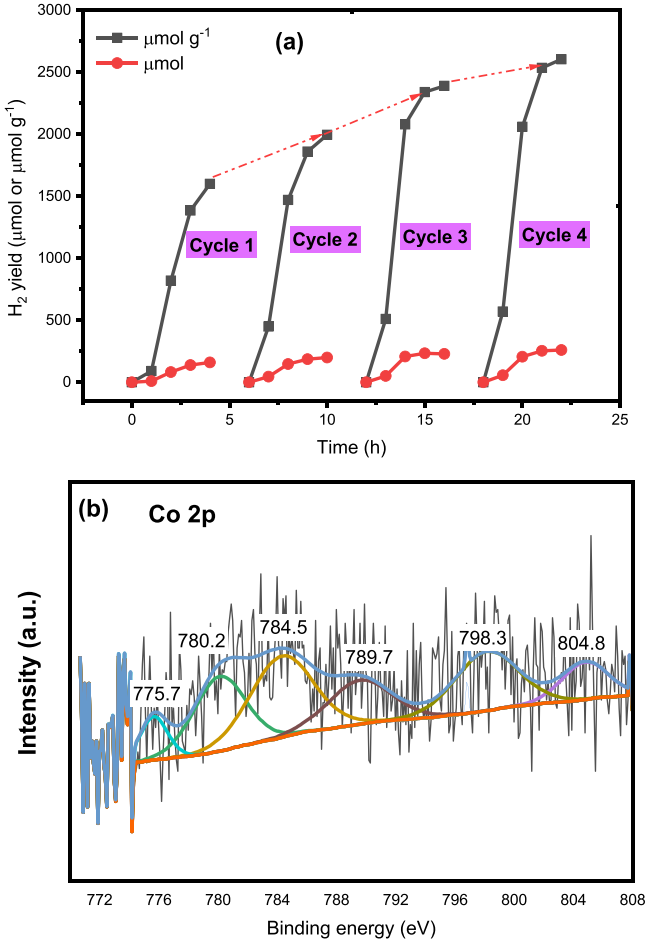

Fig. 10. (a) Cyclic test of 2% Co/HCNNR for photocatalytic production of H_2 using TEOA hole scavenger under visible light, (b) XPS analysis of used Co/HCNNR catalyst.

enhance H_2 yield. However, with increasing time, catalyst was uniformly dispersed and also, there would be exfoliation of nanorods, resulting in lower photocatalytic efficiency.

The schematic illustration for photocatalytic H_2 evolution with various catalyst loading in suspension has been illustrated in Fig. 10 (c-d). Using small amount of catalyst loading (50 mg) in 140 mL (2% TEOA), only few particles were dispersed inside the suspension. Thus, there was efficient light penetration inside suspension, however, smaller surface area was available for photoactivation, resulting in lesser amount of H_2 evolution. When the amount of catalyst was increased to 200 mg, the number of particles were increased, which created hindrance for light penetration. Due to less area of catalyst illuminated, amount of H_2 evolved per unit mass of catalyst was decreased. This reveals both the catalyst loading and light penetration inside suspension are the critical to maximize hydrogen production efficiency.

3.2.4. Stability analysis

The performance of any photocatalyst for practical application is not only dependent on the effectiveness of H_2 generation but it is also greatly relied on the recyclability and stability. The stability of Co/HCNNR was tested for consecutive four cycles using TEOA as the sacrificial reagents and the results are discussed in Fig. 10 (a). Continuous production of H_2 was evolved in all the four cycles and over the entire irradiation time. More interestingly, H_2 yield was increased after every cycle till reached to maximum value after 4th cycle. This increased in H_2 yield can be justified on several possible reasons. First, with continuous stirring of Co/HCNNR, catalyst was uniformly dispersed and exfoliated within the TEOA solution, enabling more production of protons and electrons for hydrogen production, Secondly, due to continuous light irradiation, cobalt can be reduced to metallic state, enabling it more efficient for trapping of electrons. Thirdly, during continuous light irradiation in multiple cycles, there would be possible attachment of intermediates over the photocatalyst active sites, which were also converted to hydrogen during photocatalysis process. However, further investigations are required to understand new findings in the presence of transition metal loaded 1D HCNNR and TEOA sacrificial reagent. The increased in H_2 evolution would probably be due to ability of carbon attachment to cobalt active sites, which facilitates water gas shift reaction and promotes H_2 evolution [28]. Cobalt is also well known as oxygen evolution cocatalyst with other semiconductors, which enables the utilization of carbon attached over catalyst active sites and convert to gaseous products, resulting in more active sites available for further reaction [29].

To further investigate the possible pathways of efficiency enhancement, Co/HCNNR spent catalyst was further characterized suing XPS analysis and the results are presented in Fig. 10 (b). In the resolution spectrum of Co 2p, six peaks were obtained, which were positioned at binding energies 775.7, 780.2, 784.5, 789.7, 798.3, and 804.8 eV. The peaks appeared with binding energies 775.7 and 784.5 eV reflects the presence of cobalt in metallic state (Co°). The other strong peak at 780.2 and 798.3 eV belongs to cobalt as the Co^{2+} and similarly discussed previously [56]. The two peaks at 789.7 and 804.8 eV are satellite peaks, which further confirms the existence of cobalt as oxide state [17]. Previously, Fe-Co loaded g-C_3N_4 for H_2 evolution was examined in multiple cycles, whereas, after every cycle, H_2 yield was significantly weakened [19]. Similarly, we tested stability performance of Ru/g-C_3N_4 with methanol as the sacrificial reagent, however, photocatalyst lost stability after every cycle [40]. CoP/g-C_3N_4 was tested for stability analysis, however, photoactivity for H_2 evolution was dropped after 2nd cyclic run [57]. Similarly, in another development, stability analysis for H_2 evolution over CoP/g-C_3N_4 was conducted for nine runs and reported a continuous drop in H_2 evolution. The CoP/g-C_3N_4 spent catalyst was further characterized and observed identical XRD patterns of fresh and used samples [31,50]. Ni-cluster/g-C_3N_4 was tested for H_2 production, and stability in multiple cycles was not consistent [23]. Co/TiO_2 was tested for photocatalytic H_2 evolution and reported stable photoactivity in multiple cycles [30]. All these literature findings confirm that Co not only improve active sites with improve charges separation, but also, improve photostability in multiple cycles.

3.3. Proposed mechanism for hydrogen production

The photocatalyst activity can be systematically discussed based on charge transfer within the heterostructure which is schematically discussed in Fig. 11. The 1D HCNNR provides a good interface interaction with cobalt, which enables effectual charge carrier transfer and separation with higher light energy utilization. Under solar irradiation, electron (e^-) and holes (h^+) are generated over the HCNNR surface, and then the photogenerated electron transferred along the length of nanorods, providing unidirectional flow, which limits their recombination rate. Previously, higher charge transfer over 3D DOM g-C_3N_4 was observed compared to bulk g-C_3N_4, resulting in higher charge transfer due to quantum size effect [36]. The presence of Co works as a cocatalyst and trap electrons, which are finally transferred for H^+ reduction to hydrogen. The holes retained at VB are consumed for water with the production of protons (H^+). The presence of sacrificial reagent utilized holes and hinder the recombination of photogenerated electrons and holes, whereas, improves the photocatalytic activity. Previously, it was reported that

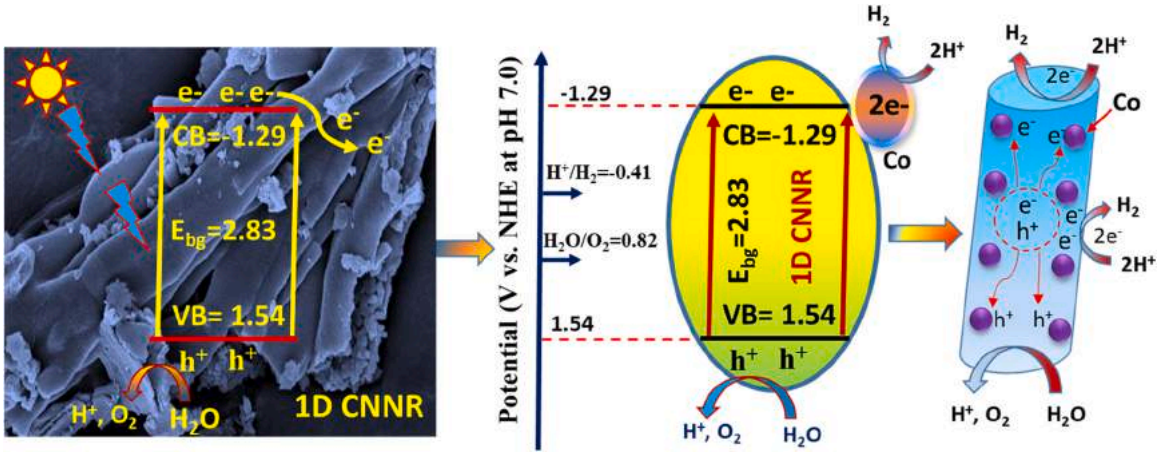

Fig. 11. Proposed charge transfer pathways for photocatalytic H_2 evolution over Co-loaded 1D HCNNR photocatalyst under visible light.

the presence of cobalt reduces overpotential of H_2 evolution and facilitates the transfer of photoinduced electrons, thus improving H_2 evolution activity [30]. Therefore, both morphology alternation and metal loading are beneficial to promote charges separation with higher light utilization for promoting photocatalytic efficiency.

4. Conclusions

In this study, template free 1D hierarchical carbon nitrides nanorods (CNNRs) imbedded with Co were successfully designed and fabricated for efficient and stable photocatalytic H_2 evolution under solar energy. The optimized 2% Co/HCNNR exhibits remarkable H_2 production of 620 µmol g^{-1}, roughly 11.27 and 17.71 folds more than it was attained with pure HCNNR and g-C_3N_4, respectively. The one-dimensional structure is beneficial to provides larger surface area for the penetration of light irradiation with higher transportation of charge carrier. The cobalt was promising to produce active sites which work as mediator to trap electrons. Thus, 1D HCNNR with cobalt as cocatalyst was not only beneficial to trap and transport electrons but they also restrain back flowing of electron and accelerates the charge transfer for H_2 production. The presence of sacrificial reagent provides boost to water splitting reaction and improves H_2 evolution kinetic. The mass transfer, number of protons in sacrificial reagents, alpha-hydrogen and viscosity of sacrificial reagents were the influential parameters to control reaction kinetics, which should be optimized to maximize photocatalyst performance for facilitating photocatalytic H_2 evolution. Using methanol and TEOA, highest hydrogen production was obtained, whereas, 2% TEOA and 5% methanol were the best concentrations to get highest H_2 evolution rate. Among the catalyst loading, more hydrogen was evolved with increasing loading amounts, however, rate per unit mass was decreased. The continuous photoactivity and stability was further achieved in consecutive four cycles with increasing trends of H_2 evolution. This study provides new approach for constructing hierarchical 1D nanorods of g-C_3N_4 for developing highly efficient photocatalyst and would be promising for other solar energy applications.

CRediT authorship contribution statement

Beenish Tahir: Methodology, Writing – original draft, Formal analysis. **Muhammad Tahir:** Financial support, Conceptualization, Supervision. **Mohammad Siraj:** Proof reading and analytical support. **Amanullah Fatehmulla:** Proof reading and analytical support.

Declaration of Competing Interest

The authors declare that they have no known competing financial interests or personal relationships that could have appeared to influence the work reported in this paper.

Acknowledgment

This work was financially supported by United Arab Emirates University (UAEU), United Arab Emirates, under Startup Research Grant (Grant # 12N097).

References

[1] S. Tasleem, M. Tahir, Z.Y. Zakaria, Fabricating structured 2D Ti_3AlC_2 MAX dispersed TiO_2 heterostructure with Ni_2P as a cocatalyst for efficient photocatalytic H_2 production, J. Alloy. Compd. 842 (2020) 155752.
[2] M. Tahir, Binary Ni_2P/Ti_3C_2 multilayer cocatalyst anchored TiO_2 nanocomposite with etchant/oxidation grown TiO_2 NPs for enhancing photocatalytic H_2 production, Energy Fuels 35 (17) (2021) 14197–14211.
[3] Y. Li, W. Zhang, H. Li, T. Yang, S. Peng, C. Kao, W. Zhang, Ni-B coupled with borate-intercalated $Ni(OH)_2$ for efficient and stable electrocatalytic and photocatalytic hydrogen evolution under low alkalinity, Chem. Eng. J. 394 (2020) 124928.
[4] M. Arumugam, M. Tahir, P. Praserthdam, Effect of nonmetals (B, O, P, and S) doped with porous g-C_3N_4 for improved electron transfer towards photocatalytic CO_2 reduction with water into CH_4, Chemosphere 286 (Pt. 2) (2021) 131765.
[5] Z. Xu, Y. Wang, J. Zhuang, Y. Li, L. Jia, High temperature hydrothermal etching of g-C_3N_4 for synthesis of N doped carbon quantum dots-supported CdS photocatalyst to enhance visible light driven hydrogen generation, Mol. Catal. 517 (2022) 111900.
[6] Z. Tian, X. Yang, Y. Chen, X. Wang, T. Jiao, W. Zhao, H. Huang, J. Hu, Construction of $LaFeO_3$/g-C_3N_4 nanosheet-graphene heterojunction with built-in electric field for efficient visible-light photocatalytic hydrogen production, J. Alloy. Compd. 890 (2022) 161850.
[7] M. Sun, Y. Zhou, T. Yu, J. Wang, Synthesis of g-C_3N_4/WO_3-carbon microsphere composites for photocatalytic hydrogen production, Int. J. Hydrog. Energy 47 (18) (2022) 10261–10276.
[8] Z. You, X. Yue, D. Zhang, J. Fan, Q. Xiang, Construction 0D/2D heterojunction by highly dispersed Ag_2S quantum dots (QDs) loaded on the g-C_3N_4 nanosheets for photocatalytic hydrogen evolution, J. Colloid Interface Sci. 607 (Pt. 1) (2022) 662–675.
[9] X. Li, J. Hu, T. Yang, X. Yang, J. Qu, C.M. Li, Efficient photocatalytic H_2-evolution coupled with valuable furfural-production on exquisite 2D/2D $LaVO_4$/g-C_3N_4 heterostructure, Nano Energy 92 (2022) 106714.
[10] Z. Chen, F. Guo, H. Sun, Y. Shi, W. Shi, Well-designed three-dimensional hierarchical hollow tubular g-C_3N_4/$ZnIn_2S_4$ nanosheets heterostructure for achieving efficient visible-light photocatalytic hydrogen evolution, J. Colloid Interface Sci. 607 (2022) 1391–1401.
[11] S. Tasleem, M. Tahir, Constructing La_xCoyO_3 perovskite anchored 3D g-C_3N_4 hollow tube heterojunction with proficient interface charge separation for stimulating photocatalytic H_2 production, Energy Fuels 35 (11) (2021) 9727–9746.
[12] S. Tasleem, M. Tahir, Synergistically improved charge separation in bimetallic Co–La modified 3D g-C_3N_4 for enhanced photocatalytic H_2 production under UV–visible light, Int. J. Hydrog. Energy 46 (40) (2021) 20995–21012.
[13] N. Fajrina, M. Tahir, Engineering approach in stimulating photocatalytic H_2 production in a slurry and monolithic photoreactor systems using Ag-bridged Z-scheme pCN/TiO_2 nanocomposite, Chem. Eng. J. 374 (2019) 1076–1095.

[14] H. Zhang, Q. Li, B. Li, B. Weng, Z. Tian, J. Yang, J. Hofkens, F. Lai, T. Liu, Atomically dispersed Pt sites on porous metal–organic frameworks to enable dual reaction mechanisms for enhanced photocatalytic hydrogen conversion, J. Catal. 407 (2022) 1–9.

[15] J. Serafin, M. Ouzzine, J. Sreńscek-Nazzal, J. Llorca, Photocatalytic hydrogen production from alcohol aqueous solutions over TiO_2-activated carbon composites decorated with Au and Pt, J. Photochem. Photobiol. A 425 (2022) 113726.

[16] W.A. Qureshi, X. Hong, X. He, Q. Liu, D. Xu, C. Maouche, Z. Sun, J. Yang, Dual plasmonic Au and TiN cocatalysts to boost photocatalytic hydrogen evolution, Chemosphere 291 (Pt. 3) (2022) 132987.

[17] Y. Chen, X. Ren, X. Wang, Z. Tian, X. Yang, J. Lu, H. Bai, T. Jiao, H. Huang, J. Hu, Construction of Ag decorated P-doped g-C_3N_4 nanosheets Schottky junction via silver mirror reaction for enhanced photocatalytic activities, Int. J. Hydrog. Energy 47 (1) (2022) 250–263.

[18] Z. Zheng, T. Wang, F. Han, Q. Yang, B. Li, Synthesis of Ni modified Au@CdS core-shell nanostructures for enhancing photocatalytic coproduction of hydrogen and benzaldehyde under visible light, J. Colloid Interface Sci. 606 (2022) 47–56.

[19] R. Yang, J. Liu, B. Wang, R. Wang, Y. Song, Y. Hua, C. Wang, Y. She, J. Yuan, H. Xu, H. Li, Synergistic effect of isolated Co and Fe dual active sites boosting the photocatalytic hydrogen evolution reaction, J. Alloy. Compd. 895 (2022) 162290.

[20] Y. Li, R. Tong, W. Zhang, S. Peng, Pre-intercalation of phosphate into $Ni(OH)_2$/NiOOH for efficient and stable electrocatalytic oxygen evolution reaction, J. Catal. 410 (2022) 22–30.

[21] Y. Li, T. Yang, H. Li, R. Tong, S. Peng, X. Han, Transformation of Fe-B@Fe into Fe-B@Ni for efficient photocatalytic hydrogen evolution, J. Colloid Interface Sci. 578 (2020) 273–280.

[22] F. Sarwar, M. Tahir, H. Alias, Synergistic effect of photo-reduced Ni–Ag loaded g-C_3N_4 nanosheets for efficient visible light-driven photocatalytic hydrogen evolution, Mater. Sci. Semicond. Process. 137 (2022) 106187.

[23] L. Jian, H. Zhang, B. Liu, C. Pan, Y. Dong, G. Wang, J. Zhong, Y. Zheng, Y. Zhu, Monodisperse Ni-clusters anchored on carbon nitride for efficient photocatalytic hydrogen evolution, Chin. J. Catal. 43 (2) (2022) 536–545.

[24] M. Tahir, Ni/MMT-promoted TiO_2 nanocatalyst for dynamic photocatalytic H_2 and hydrocarbons production from ethanol-water mixture under UV-light, Int. J. Hydrog. Energy 42 (47) (2017) 28309–28326.

[25] P. Yang, R. Wang, H. Tao, Y. Zhang, M.-M. Titirici, X. Wang, Cobalt nitride anchored on nitrogen-rich carbons for efficient carbon dioxide reduction with visible light, Appl. Catal. B 280 (2021) 119454.

[26] W.K. Fan, M. Tahir, Recent advances on cobalt metal organic frameworks (MOFs) for photocatalytic CO_2 reduction to renewable energy and fuels: a review on current progress and future directions, Energy Convers. Manag. 253 (2022) 115180.

[27] Z. An, W. Wang, S. Dong, J. He, Well-distributed cobalt-based catalysts derived from layered double hydroxides for efficient selective hydrogenation of 5-hydroxymethyfurfural to 2,5-methylfuran, Catal. Today 319 (2019) 128–138.

[28] T. Abbas, M. Tahir, Tri-metallic Ni–Co modified reducible TiO_2 nanocomposite for boosting H_2 production through steam reforming of phenol, Int. J. Hydrog. Energy 46 (13) (2021) 8932–8949.

[29] T. Di, B. Zhu, J. Zhang, B. Cheng, J. Yu, Enhanced photocatalytic H_2 production on CdS nanorod using cobalt-phosphate as oxidation cocatalyst, Appl. Surf. Sci. 389 (2016) 775–782.

[30] W. Chen, M. Liu, Y. Wang, L. Gao, H. Dang, L. Mao, Non-noble metal Co as active sites on TiO_2 nanorod for promoting photocatalytic H_2 production, Mater. Res. Bull. 116 (2019) 16–21.

[31] S. Peng, X. Huang, Y. Cao, J. Zuo, Y. Huang, J. Xu, Y. Li, Modification of carbon nitride with noble-metal-free cobalt phosphide for effective photocatalytic hydrogen evolution, Appl. Surf. Sci. 584 (2022) 152610.

[32] G. Huang, G. Lin, Q. Niu, J. Bi, L. Wu, Covalent triazine-based frameworks confining cobalt single atoms for photocatalytic CO_2 reduction and hydrogen production, J. Mater. Sci. Technol. 116 (2022) 41–49.

[33] W. Xing, Y. Zhang, J. Zou, T. Zhang, C. Liu, G. Wu, G. Chen, Sulfur-doped 2D/3D carbon nitride-based van der Waals homojunction with superior photocatalytic hydrogen evolution and wastewater purification, Int. J. Hydrog. Energy 47 (25) (2022) 12559–12568.

[34] C. Peng, L. Han, J. Huang, S. Wang, X. Zhang, H. Chen, Comprehensive investigation on robust photocatalytic hydrogen production over C_3N_5, Chin. J. Catal. 43 (2) (2022) 410–420.

[35] L. Liang, L. Shi, F. Wang, H. Wang, P. Yan, Y. Cong, L. Yao, Z. Yang, W. Qi, g-C_3N_4 nano-fragments as highly efficient hydrogen evolution photocatalysts: Boosting effect of nitrogen vacancy, Appl. Catal. A Gen. 599 (2020) 117618.

[36] X. Wang, Q. Li, Q. Lin, R. Zhang, M. Ding, CdS-sensitized 3D ordered macroporous g-C_3N_4 for enhanced visible-light photocatalytic hydrogen generation, J. Mater. Sci. Technol. 111 (2022) 204–210.

[37] W. Shi, W. Sun, Y. Liu, X. Li, X. Lin, F. Guo, Y. Hong, Onion-ring-like g-C_3N_4 modified with Bi_3TaO_7 quantum dots: a novel 0D/3D S-scheme heterojunction for enhanced photocatalytic hydrogen production under visible light irradiation, Renew. Energy 182 (2022) 958–968.

[38] L. Jiang, Y. Guo, J. Pan, J. Zhao, Y. Ling, Y. Xie, Y. Zhou, J. Zhao, N, P, O co-doped carbon filling into carbon nitride microtubes to promote photocatalytic hydrogen production, Sci. Total Environ. 809 (2022) 151114.

[39] X. Wang, Q. Li, L. Gan, X. Ji, F. Chen, X. Peng, R. Zhang, 3D macropore carbon-vacancy g-C_3N_4 constructed using polymethylmethacrylate spheres for enhanced photocatalytic H_2 evolution and CO_2 reduction, J. Energy Chem. 53 (2021) 139–146.

[40] B. Tahir, M. Tahir, M.G.M. Nawawai, A.H. Khoja, B.U. Haq, W. Farooq, Ru-embedded 3D g-C_3N_4 hollow nanosheets (3D CNHNS) with proficient charge transfer for stimulating photocatalytic H_2 production, Int. J. Hydrog. Energy 46 (55) (2021) 27997–28010.

[41] B. Tahir, M. Tahir, N.A.S. Amin, Ag-La loaded protonated carbon nitrides nanotubes (pCNNT) with improved charge separation in a monolithic honeycomb photoreactor for enhanced bireforming of methane (BRM) to fuels, Appl. Catal. B 248 (2019) 167–183.

[42] A.A. Khan, M. Tahir, A.R. Mohamed, Constructing S-scheme heterojunction of carbon nitride nanorods (g-CNR) assisted trimetallic CoAlLa LDH nanosheets with electron and holes moderation for boosting photocatalytic CO_2 reduction under solar energy, Chem. Eng. J. 433 (2022) 133693.

[43] Y. Li, Z. Liu, Z. Li, Q. Wang, Renewable biomass-derived carbon-supported g-C_3N_4 doped with Ag for enhanced photocatalytic reduction of CO_2, J. Colloid Interface Sci. 606 (Pt. 2) (2022) 1311–1321.

[44] Z. Zhang, Y. Zheng, H. Xie, J. Zhao, X. Guo, W. Zhang, Q. Fu, S. Wang, Q. Xu, Y. Huang, Synthesis of g-C_3N_4 microrods with superficial C, N dual vacancies for enhanced photocatalytic organic pollutant removal and H_2O_2 production, J. Alloy. Compd. 904 (2022) 164028.

[45] Y. Zhu, X. Zhong, X. Jia, J. Yao, Bimetallic Ni-Co nanoparticles confined within nitrogen defective carbon nitride nanotubes for enhanced photocatalytic hydrogen production, Environ. Res. 203 (2022) 111844.

[46] Y. Zhou, M. Sun, T. Yu, J. Wang, 3D g-C_3N_4/WO_3/biochar/Cu^{2+}-doped carbon spheres composites: synthesis and visible-light-driven photocatalytic hydrogen production, Mater. Today Commun. 30 (2022) 103084–103558.

[47] L. Wang, Y. Dong, J. Zhang, F. Tao, J. Xu, Construction of NiO/g-C_3N_4 p-n heterojunctions for enhanced photocatalytic CO_2 reduction, J. Solid State Chem. 308 (2022) 122878.

[48] L. Liang, L. Shi, F. Wang, L. Yao, Y. Zhang, W. Qi, Synthesis and photo-catalytic activity of porous g-C_3N_4: promotion effect of nitrogen vacancy in H_2 evolution and pollutant degradation reactions, Int. J. Hydrog. Energy 44 (31) (2019) 16315–16326.

[49] Y. Liu, Y. Zhang, L. Shi, One-step synthesis of S-doped and nitrogen-defects co-modified mesoporous g-C_3N_4 with excellent photocatalytic hydrogen production efficiency and degradation ability, Colloids Surf. A Physicochem. Eng. Asp. 641 (2022) 128577.

[50] S. Peng, Y. Cao, F. Zhou, Z. Xu, Y. Li, CoP decorated with Co_3O_4 as a cocatalyst for enhanced photocatalytic hydrogen evolution via dye sensitization, Appl. Surf. Sci. 487 (2019) 315–321.

[51] Y. Li, H. Li, Y. Li, S. Peng, Y.H. Hu, Fe-B alloy coupled with Fe clusters as an efficient cocatalyst for photocatalytic hydrogen evolution, Chem. Eng. J. 344 (2018) 506–513.

[52] L. Liang, L. Shi, F. Wang, H. Wang, W. Qi, The improvement of photocatalytic performance for hydrogen evolution over mesoporous g-C_3N_4 modified with nitrogen defects, Sustain. Energy Fuels 4 (10) (2020) 5179–5187.

[53] M. Tahir, Investigating the influential effect of etchant time in constructing 2D/2D HCN/MXene heterojunction with controlled growth of TiO_2 NPs for stimulating photocatalytic H_2 production, Energy Fuels 35 (8) (2021) 6807–6822.

[54] V. Kumaravel, M. Imam, A. Badreldin, R. Chava, J. Do, M. Kang, A. Abdel-Wahab, Photocatalytic hydrogen production: role of sacrificial reagents on the activity of oxide, carbon, and sulfide catalysts, Catalysts 9 (3) (2019) 276.

[55] S. Tasleem, M. Tahir, Investigating the performance of liquid and gas phase photoreactors for dynamic H_2 production over bimetallic TiO_2 and Ni_2P dispersed MAX Ti_3AlC_2 monolithic nanocomposite under UV and visible light, J. Environ. Chem. Eng. 9 (4) (2021) 105351.

[56] Z. Wang, F. Wang, K. Liu, J. Zhu, T. Chen, Z. Gu, S. Yin, Cobalt phosphide nanoparticles grown on Ti_3C_2 nanosheet for enhanced lithium ions storage performances, J. Alloy. Compd. 853 (2021) 157136.

[57] X. Liu, Y. Xu, Y. Jiang, M. Song, Z. Liu, W. Guo, L. You, J. Wu, M. Xu, Y. He, Nanoarchitectonics of uniformly distributed noble-metal-free CoP in g-C_3N_4 via in-situ fabrication for enhanced photocatalytic and electrocatalytic hydrogen production, J. Alloy. Compd. 904 (2022) 163861.